Stable, high order accurate adaptive schemes for long time, highly intermittent geophysics problems

Brittany A. Erickson [a,*], Jan Nordström [b]

[a] Department of Geological Sciences, San Diego State University, San Diego, CA 92182-1020, USA
[b] Department of Mathematics, Division of Computational Mathematics, Linköping University, SE-581 83 Linköping, Sweden

ARTICLE INFO

ABSTRACT

Many geophysical phenomena are characterized by properties that evolve over a wide range of scales which introduce difficulties when attempting to model these features in one computational method. We have developed a high-order finite difference method for the elastic wave equation that is able to efficiently handle varying temporal and spatial scales in a single, stand-alone framework. We apply this method to earthquake cycle models characterized by extremely long interseismic periods interspersed with abrupt, short periods of dynamic rupture. Through the use of summation-by-parts operators and weak enforcement of boundary conditions we derive a provably stable discretization. Time stepping is achieved through the implicit θ-method which allows us to take large time steps during the intermittent period between earthquakes and adapts appropriately to fully resolve rupture.

© 2014 Elsevier B.V. All rights reserved.

1. Introduction

Earthquake rupture is one example of many geophysical phenomena that are characterized by properties that evolve over many orders of magnitude in both time and space. Modeling these phenomena with full temporal and spatial resolution is thus quite difficult and it is often the case that simplifying assumptions are made in numerical studies. Because the initial conditions prior to an earthquake are not well understood, many studies of earthquake rupture for example, impose artificial initial conditions in the form of a stress perturbation in order to immediately nucleate dynamic rupture [1–3]. These methods capture the fine details of the rupture process and wave propagation, but are limited to single-earthquake simulations without realistic initial data.

Obtaining self-consistent initial conditions would require modeling the interseismic loading period prior to rupture, but this is computationally infeasible with the explicit time-stepping techniques generally used. Since stability considerations with explicit methods limit the size of the time step to fractions of a second, these methods are not appropriate for modeling the tectonic loading period characterized by tens to hundreds of years. In order to model full earthquake cycles however, these multiple time scales have been handled with several different techniques. The methods of [4] and [5] involve an abrupt switching between solving the static problem (in which inertia is neglected) and the dynamic problem. The method in [6] disregard inertia entirely and assume that the rupture is quasi-dynamic and therefore do not simulate wave propagation. The authors of [7] present a method that is able to simulate long interseismic periods punctuated by dynamic events within one computational framework, but the method is based on the boundary integral method and make the simplifying assumption of rupture occurring in a homogeneous, linear elastic whole or half-space.

---

* Corresponding author. Tel.: +1 7072873188.
  E-mail addresses: brittanya.erickson@gmail.com, berickson@mail.sdsu.edu (B.A. Erickson), jan.nordstrom@liu.se (J. Nordström).
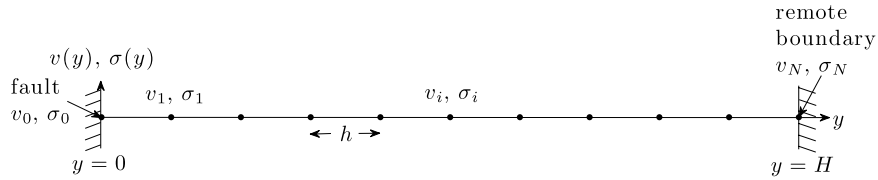
Fig. 1. Physical and computational setting for 1D elastic wave equation in first order form on an unstaggered grid. The system, initially essentially at rest, is loaded at the remote boundary $y = H$ by a velocity boundary condition intended to capture the effect of slow tectonic loading. Periodic earthquakes nucleate at the fault, which lies at the boundary $y = 0$ and is governed by a stress boundary condition. The domain is discretized at $N + 1$ points with grid spacing $h = H/N$.

In this work we simulate both the interseismic period and fully dynamic rupture in one-computational setting, with a volume discretization which allows the method to incorporate variable material properties. The method applies high order finite difference operators which provide an efficient approach, and yields a semi-discrete problem which is provably stable. The efficiency can be used either to increase the accuracy for a fixed number of mesh points or to reduce the computational cost for a given accuracy by reducing the number of mesh points [8,9]. In the past, the main drawback with high order finite difference methods was the complicated boundary treatment required to obtain a stable method. However, the development during the last two decades has removed this obstacle. Finite difference operators which satisfy the summation-by-parts (SBP) property [10–12], are central difference operators in the interior domain augmented with special stencils near the domain boundaries. These SBP operators in combination with weak well-posed boundary conditions lead to energy stability [13–19]. The preferred boundary treatment is the simultaneous approximation term (SAT) method [20], which linearly combines the partial differential equation to be solved with well-posed boundary conditions [21,13,22,23]. A complete description of the SBP–SAT method is given in the review article [24].

Time-stepping is done through the implicit θ-method which yields a first or second-order accurate (in time) method and is A-stable [25]. The time step adapts according to an estimate of the local truncation error, and can be quite large during the interseismic period while still maintaining stability. Although the main drawback compared to explicit methods is that a nonlinear system of equations must be solved at every time step, efficiency is gained by the ability to take large time steps, and we make no simplifying assumption of inertia being negligible during the interseismic period. Through this technique we obtain self-consistent initial conditions prior to rupture which reflect many years of tectonic loading. In this initial development we focus on the development of an efficient and stable time-stepping method for a high-order accurate spatial discretization. We consider the one-dimensional problem which contains all of the difficulties present in the multi-dimensional problem (such as varying temporal and spatial scales, and extreme stiffness), while providing the simplest possible framework in which to introduce the method. The extension to multi-dimensions is straight forward.

2. Continuous formulation and well-posedness

2.1. Preliminaries

We simulate multiple earthquake cycles where events nucleate at a frictional fault at one boundary of the domain. The material off the fault is governed by the elastic wave equation in first order form, see Fig. 1. In addition to the varying time scales governing geophysical phenomena, as described in the introduction, there are also computational challenges introduced through varying spatial scales. Faults can be hundreds of kilometers long, with frictional properties on the order of microns. These features often lead to very large problems in order to fully resolve multiple length scales.

2.2. Governing equations and well-posedness via the energy method

Assuming linear elasticity in first order form, the governing equations and boundary conditions are:

$$\frac{\partial w}{\partial t} = B\frac{\partial w}{\partial y}, \quad B = \begin{bmatrix} 0 & 1/\rho \\ \mu & 0 \end{bmatrix}, \quad w = \begin{bmatrix} v \\ \sigma \end{bmatrix}, \quad y \in [0, H] \tag{2.1a}$$

$$L_o(w) = \sigma(0, t) = F(V(t)), \qquad L_1(w) = v(H, t) = V_p. \tag{2.1b}$$

The parameters ρ and μ are the material density and shear modulus and the boundary operators L_o and L_1 act on the shear stress σ and particle velocity v, respectively. We assume that a frictional fault lies at $y = 0$ and is governed by a boundary condition that equates shear stress with fault strength given through an experimentally-motivated friction law F dependent on the particle velocity at the fault $V(t) = v(0, t)$ (known as the "slip velocity"), discussed in Section 4.3. The system is initially at rest and undergoes an interseismic period where it is loaded at the remote boundary. We set the velocity at the remote boundary $y = H$ to a slow "plate rate" V_p, intended to capture the effect of slow tectonic loading. Measurements of typical values of V_p are around 32 mm/a (e.g. the San Andreas Fault in southern California). This remote boundary condition will load the system and increase the stress at the fault, which will eventually cause earthquakes to initiate at the fault, sending waves through the medium.

To analyze problem (2.1) we symmetrize the equations to

$$\frac{\partial u}{\partial t} = A\frac{\partial u}{\partial y}, \quad A = \begin{bmatrix} 0 & c_s \\ c_s & 0 \end{bmatrix}, \quad u = W^{-1}w = \left[\sqrt{\frac{\rho}{2}}v, \frac{1}{\sqrt{2\mu}}\sigma\right]^T, \tag{2.2}$$

where $c_s = \sqrt{\mu/\rho}$ is the shear wave speed and $B = WAW^{-1}$, $W = \text{diag}(\sqrt{2/\rho}, \sqrt{2\mu})$. The eigenvalues of A are $\pm c_s$, which imply that one boundary condition is required at each end of the domain.

The non-conventional nonlinear boundary condition in (2.1b) forces a check of well-posedness, see [26,27]. Letting $||\cdot||$ denote the standard L^2 norm we may now consider the total mechanical energy of the system $||u||^2$ as a sum of the kinetic and strain energies. Taking the data $V_p = 0$, the energy method applied to Eq. (2.2) yields

$$\frac{d}{dt}\|u\|^2 = 2\int_0^H u^T A u \, dy = 2c_s u_1 u_2|_0^H = v\sigma|_0^H = -VF(V) \leq 0, \tag{2.3}$$

with the assumption that the friction law F has the physically relevant property that it takes the sign of its argument, i.e. $F(V)V \geq 0$.

Uniqueness is obtained by considering the difference problem of the form (2.2), i.e.

$$\frac{\partial \Delta u}{\partial t} = A\frac{\partial \Delta u}{\partial y} \tag{2.4}$$

where $\Delta u = u - \hat{u}$ is the difference between two solutions satisfying the boundary conditions $\Delta u_1(H, t) = 0$ and $\Delta u_2(0, t) = \frac{1}{\sqrt{2\mu}}(F(V) - F(\hat{V}))$.

The energy method thus yields:

$$\frac{d}{dt}\|\Delta u\|^2 = 2\int_0^H \Delta u^T A \Delta u \, dy = 2c_s(u_1 - \hat{u}_1)(u_2 - \hat{u}_2)\Big|_0^H$$
$$= -(V - \hat{V})(F(V) - F(\hat{V})) = -\Delta V^2 F'(V^*) \leq 0, \tag{2.5}$$

where $V \leq V^* \leq \hat{V}$ and the intermediate value theorem is applied. We can summarize this result in the following proposition [26]:

Proposition 1. *The problem* (2.1) *is well-posed if the friction law F in* (2.1) *satisfies* $VF(V) \geq 0$ *and* $F'(V) \geq 0$.

3. Spatial discretization and stability

3.1. Semi-discretization

For the discrete problem we will make use of the Kronecker product

$$A \otimes B := \begin{bmatrix} a_{0,0}B & \cdots & a_{0,N}B \\ \vdots & & \vdots \\ a_{N,0}B & \cdots & a_{N,N}B \end{bmatrix}$$

which has the following properties:

$$(A \otimes B)^T = (A^T \otimes B^T), \qquad (A \otimes B)^{-1} = (A^{-1} \otimes B^{-1}), \qquad A \otimes (B + C) = (A \otimes B) + (A \otimes C).$$

We discretize (2.1) using high-order summation-by-parts (SBP) finite difference operators for first derivatives [28]. The boundary conditions are imposed weakly through the simultaneous-approximation-term (SAT) [20] which penalizes the solution at the boundaries for not satisfying the boundary conditions.

The semi-discrete form of Eqs. (2.1) using the SBP–SAT framework is

$$(P \otimes I_2)\mathbf{w}_t = (Q \otimes B)\mathbf{w} + \left(e_0 \otimes \Sigma_0 \begin{bmatrix} \sigma_0 - F(v_0) \\ \sigma_0 - F(v_0) \end{bmatrix}\right) + \left(e_N \otimes \Sigma_N \begin{bmatrix} v_N - V_p \\ v_N - V_p \end{bmatrix}\right) \tag{3.1}$$

where bold quantities refer to grid vectors: $\mathbf{w} = [v_0, \sigma_0, v_1, \sigma_1, \ldots, v_N, \sigma_N]^T$ and I_2 is a 2×2 identity matrix. We will often refer to the vector $w_i = [v_i, \sigma_i]^T$, $i = 0, \ldots, N$. The operators P and Q are building blocks that form the finite difference SBP operator $\partial/\partial y \approx P^{-1}Q$ where P is a matrix norm defining the discrete norm $\|\mathbf{u}\|_P^2 = \mathbf{u}^T P\mathbf{u}$ for any grid vector $\mathbf{u}$. The 2×2 matrices Σ_0 and Σ_N are penalty matrices that enforce the boundary conditions weakly

$$\Sigma_0 := \begin{bmatrix} \delta_1 & 0 \\ 0 & \delta_1 \end{bmatrix}, \qquad \Sigma_N := \begin{bmatrix} \delta_3 & 0 \\ 0 & \delta_4 \end{bmatrix}. \tag{3.2}$$

We symmetrize the matrix $B = WAW^{-1}$ as before. By letting I_N denote the $N \times N$ identity matrix, Eq. (3.1) becomes

$$(P \otimes I_2) \mathbf{u}_t = (Q \otimes A) \mathbf{u} + \left(e_0 \otimes \tilde{\Sigma}_0 \begin{bmatrix} \sigma_0 - F(v_0) \\ \sigma_0 - F(v_0) \end{bmatrix} \right) + \left(e_N \otimes \tilde{\Sigma}_N \begin{bmatrix} v_N - V_p \\ v_N - V_p \end{bmatrix} \right) \tag{3.3}$$

where $\tilde{\Sigma}_0 = W^{-1}\Sigma_0$, $\tilde{\Sigma}_N = W^{-1}\Sigma_N$ and $\mathbf{u} = (I_N \otimes W^{-1}) \mathbf{w}$ is the scaled vector of grid data,

$$\mathbf{u} = (I_N \otimes W^{-1}) \mathbf{w} = \left[\sqrt{\rho/2} v_o, (1/\sqrt{2\mu})\sigma_o, \ldots, \sqrt{\rho/2}\, v_N, (1/\sqrt{2\mu})\sigma_N \right]^T \tag{3.4}$$

which allows us to consider the total semi-discrete energy of the system

$$\mathbf{E} = ||\mathbf{u}||^2_{P \otimes I_2}. \tag{3.5}$$

3.2. Semi-discrete stability via discrete energy method

The penalty matrices $\tilde{\Sigma}_0$ and $\tilde{\Sigma}_N$ will be determined such that we get a discrete energy estimate. We will also make use of matrices C_0 and C_N in order to map vectors $[v_{0,N}, v_{0,N}]^T$ and $[\sigma_{0,N}, \sigma_{0,N}]^T$ back to $w_{0,N}$. We define

$$C_0 = \begin{bmatrix} 0 & 1 \\ 0 & 1 \end{bmatrix} \quad \text{and} \quad C_N = \begin{bmatrix} 1 & 0 \\ 1 & 0 \end{bmatrix}, \tag{3.6}$$

so that

$$C_0 w_{0,N} = \begin{bmatrix} \sigma_{0,N} \\ \sigma_{0,N} \end{bmatrix} = C_0 W u_{0,N} \quad \text{and} \quad C_N w_{0,N} = \begin{bmatrix} v_{0,N} \\ v_{0,N} \end{bmatrix} = C_N W u_{0,N}. \tag{3.7}$$

By multiplying Eq. (3.3) by $\mathbf{u}^T$ and adding the transpose, we obtain

$$\frac{d}{dt} ||\mathbf{u}||^2_{P \otimes I_2} = \mathbf{u}^T \left[(Q + Q^T) \otimes A \right] \mathbf{u} + \mathbf{u}_0^T \left(\tilde{\Sigma}_0 \begin{bmatrix} \sigma_0 - F(v_0) \\ \sigma_0 - F(v_0) \end{bmatrix} \right) + \left(\tilde{\Sigma}_0 \begin{bmatrix} \sigma_0 - F(v_0) \\ \sigma_0 - F(v_0) \end{bmatrix} \right)^T \mathbf{u}_0$$

$$+ \mathbf{u}_N^T \left(\tilde{\Sigma}_N \begin{bmatrix} v_N - V_p \\ v_N - V_p \end{bmatrix} \right) + \left(\tilde{\Sigma}_N \begin{bmatrix} v_N - V_p \\ v_N - V_p \end{bmatrix} \right)^T \mathbf{u}_N. \tag{3.8}$$

Using the fact that Q is almost skew-symmetric and taking $V_p = 0$, Eq. (3.8) simplifies to:

$$\frac{d}{dt} ||\mathbf{u}||^2_{P \otimes I_2} = -u_0^T A u_0 + u_N^T A u_N + u_0^T W^{-1} \Sigma_0 C_0 W u_0 - u_0^T W^{-1} \Sigma_0 [F(v_0)\, F(v_0)]^T$$

$$+ u_0^T W^T C_0^T \Sigma_0^T (W^{-1})^T u_0 - [F(v_0)\, F(v_0)] \Sigma_0^T (W^{-1})^T u_0 + u_N^T W^{-1} \Sigma_N C_N W u_N$$

$$+ u_N^T W^T C_N^T \Sigma_N^T (W^{-1})^T u_N \tag{3.9}$$

where matrices C_0, C_N are given by (3.7). Collecting terms yields

$$\frac{d}{dt} ||\mathbf{u}||^2_{P \otimes I_2} = -u_0^T [A - W^{-1} \Sigma_0 C_0 W - W^T C_0^T \Sigma_0^T (W^{-1})^T] u_0$$

$$+ u_N^T [A + W^{-1} \Sigma_N C_N W + W^T C_N^T \Sigma_N^T (W^{-1})^T] u_N$$

$$- u_0^T W^{-1} \Sigma_0 [F(v_0)\, F(v_0)]^T - [F(v_0)\, F(v_0)] \Sigma_0^T (W^{-1})^T u_0 \tag{3.10}$$

which we can express as

$$\frac{d}{dt} ||\mathbf{u}||^2_{P \otimes I_2} = -u_0^T \begin{bmatrix} 0 & c_s - Z\delta_1 \\ c_s - Z\delta_1 & -2\delta_2 \end{bmatrix} u_0 + u_N^T \begin{bmatrix} 2\delta_3 & c_s + \delta_4/Z \\ c_s + \delta_4/Z & 0 \end{bmatrix} u_N$$

$$- u_0^T W^{-1} \Sigma_0 [F(v_0)\, F(v_0)]^T - [F(v_0)\, F(v_0)] \Sigma_0^T (W^{-1})^T u_0 \tag{3.11}$$

where $Z = \sqrt{\rho\mu}$ is the shear impedance and $\delta_1, \delta_2, \delta_3, \delta_4$ correspond to the penalty matrices defined in (3.2). Taking

$$\delta_1 = 1/\rho, \qquad \delta_2 = 0, \qquad \delta_3 = 0 \quad \text{and} \quad \delta_4 = -\mu \tag{3.12}$$

Eq. (3.11) simplifies to

$$\frac{d}{dt} ||\mathbf{u}||^2_{P \otimes I_2} = -w_0^T (W^{-1})^T W^{-1} \Sigma_0 [F(v_0)\, F(v_0)]^T - [F(v_0)\, F(v_0)] \Sigma_0^T (W^{-1})^T W^{-1} w_0$$

$$= -v_0 F(v_0) \leq 0, \tag{3.13}$$

which is the discrete analog to estimate (2.3). We can summarize the result in the following proposition:

Proposition 2. *The semi-discrete Eq.* (3.1) *with the penalty matrices determined by* (3.12) *is a stable approximation of* (2.1).
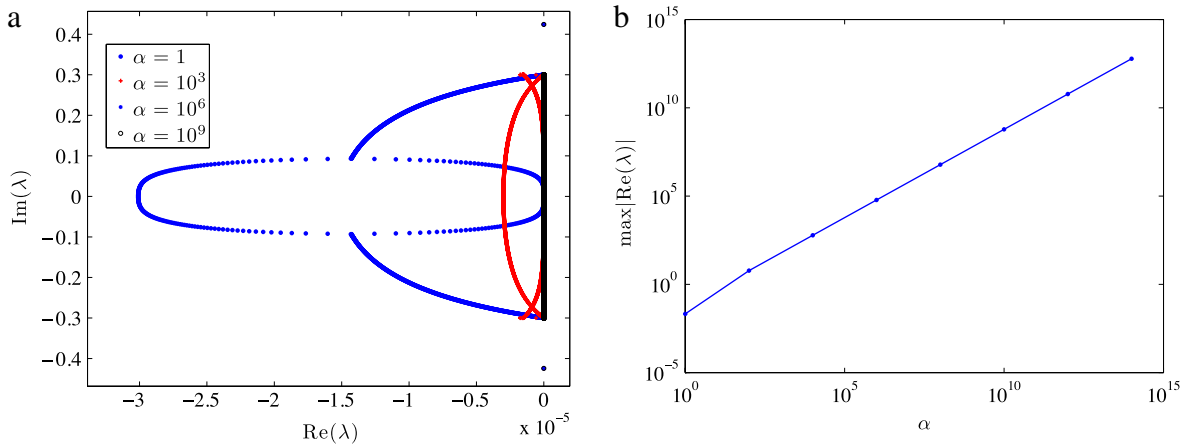
Fig. 2. (a) Most of the eigenvalues of J for $\alpha = 1$, 1e3, 1e6, 1e9 lie on or near the imaginary axis, characteristic of hyperbolic PDEs. Not visible in (a) is the eigenvalue with largest (in magnitude) real part shown in (b) whose real part tends towards $-\infty$ with increasing α.

4. Time stepping

4.1. Preliminaries

For a preliminary analysis on which time stepping method to use, we consider a linear friction law of the form $F(v_0) = \alpha v_0$. This allows us to express Eq. (3.1) as

$$\mathbf{w}_t = E\mathbf{w}. \tag{4.1}$$

We diagonalize matrix $E = X^{-1}\Lambda X$, where the diagonal matrix Λ stores the eigenvalues of E. Thus (4.1) can be expressed as $\mathbf{y}_t = \Lambda \mathbf{y}$ (where $\mathbf{y} = X\mathbf{w}$) which has the solution $\mathbf{y}(t) = e^{\Lambda t}\mathbf{y}_0$, where $\mathbf{y}_0$ is the initial condition. Thus the eigenvalues of E must have negative real part for the ODE (4.1) to be stable. The explicit form of Eq. (4.1) with zero boundary data is

$$\mathbf{w}_t = (P \otimes I_2)^{-1} \left[Q \otimes B + E_0 \otimes \left(\Sigma_0 \begin{bmatrix} -\alpha & 1 \\ -\alpha & 1 \end{bmatrix} \right) + E_N \otimes \left(\Sigma_N \begin{bmatrix} 1 & 0 \\ 1 & 0 \end{bmatrix} \right) \right] \mathbf{w} \tag{4.2}$$

where the value of α influences the eigenvalues of the Jacobian matrix of system (4.2):

$$J = \frac{\partial E}{\partial \mathbf{w}} = (P \otimes I_2)^{-1} \left[Q \otimes B + E_0 \otimes \left(\Sigma_0 \begin{bmatrix} -\alpha & 1 \\ -\alpha & 1 \end{bmatrix} \right) + E_N \otimes \left(\Sigma_N \begin{bmatrix} 1 & 0 \\ 1 & 0 \end{bmatrix} \right) \right]. \tag{4.3}$$

In [26] it was found that α/Z can range over tens of orders of magnitude during a single earthquake rupture and leads to numerical stiffness. As Fig. 2 shows, if the friction law exhibits a linear relationship with slip velocity through a coefficient α which varies temporally over many orders of magnitude, then the Jacobian matrix J will have an eigenvalue with increasingly large negative real part. Thus, in order to not have to take prohibitively small time steps, our time stepping scheme should be both implicit and A-stable (the region of absolute stability contains the left half of the complex plane).

4.2. θ-method

The θ-method for solving a general ODE given by $u' = g(t, u)$ is given by

$$\frac{u^n - u^{n-1}}{\Delta t} = \theta g(t^n, u^n) + (1 - \theta)g(t^{n-1}, u^{n-1}).$$

For $\theta = 1$ we have the 1st order backward Euler formula, and $\theta = 1/2$ corresponds to the 2nd order trapezoidal method. Both methods are implicit, A-stable, and the backward-Euler method is also L-stable (an A-stable method where, when applied to the test equation $y' = \lambda y$, the amplification factor $\to 0$ as $\Delta t\lambda \to \infty$. See [25]). We apply the backward-Euler method ($\theta = 1$) for its desirable stability properties. To derive an adaptive backward-Euler method we compare the first order approximation with that of a higher order method. Thus two numerical approximations to the solution are computed at each time step with both $\theta = 1$ and $\theta = 1/2$. The norm of the error made between the first ($\theta = 1$) and second order ($\theta = 1/2$) accurate solutions yield an estimate EST to the local truncation error. The error estimate is used to decide whether to accept the results from the first order method, or to redo the step with a smaller step size, according to whether or not $EST < ETOL$, a desired integration tolerance. Therefore the resulting method has a discontinuous change in time step. For a
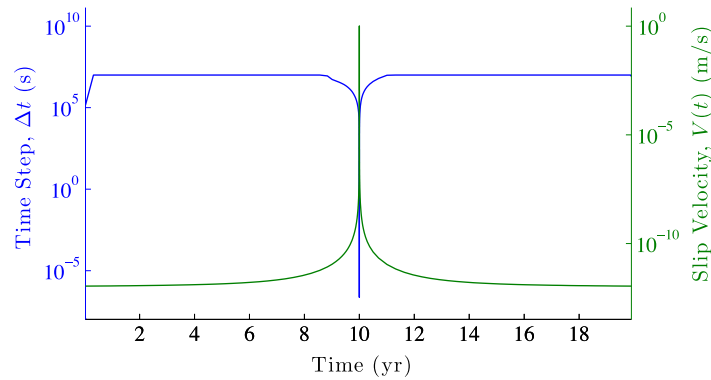
Fig. 3. Time step and slip velocity as a function of time for the manufactured solution. Time steps (blue) are quite large while slip velocity $V(t)$ (green) remains around v_{min} for a 10 year interseismic loading period. At $\bar{t} = 10$ years, a dynamic "event" occurs where the slip velocity increases over 10 orders of magnitude to a value v_{max} over the time scale t_w. Parameters used in this simulation are given in Table 1. We allow Δt to be as large as 10^7 seconds ∼several months, and it adapts accordingly during the event (decreasing to values on the order of fractions of a second) in order to resolve rupture. (For interpretation of the references to color in this figure legend, the reader is referred to the web version of this article.)

method of order p, the new step size $h_{n+1} = rh_n$ is chosen conservatively so that the estimated error is a fraction of *ETOL*, $|r^{p+1}EST| = frac\ ETOL$, with $frac = 0.9$, for example. Thus

$$r = \left(\frac{frac\ ETOL}{EST}\right)^{\frac{1}{p+1}}$$

determines the next time step, see [25] for more details.

4.3. The friction law

The specific form of the friction law we use is the aging law in rate-and-state friction [29–32], where the shear stress on the fault $\tau(t) = \sigma(0, t)$ is equated with fault strength

$$\tau = F(V, \psi), \tag{4.4}$$

where fault strength F is the normal stress σ_n times the friction coefficient f. In the rate-and-state framework, the fault strength is a function of slip velocity $V(t) = v(0, t)$ and a state variable ψ in the following form:

$$F(V, \psi) = \sigma_n f(V, \psi) = \sigma_n a \sinh^{-1}\left(\frac{V}{2V_0}e^{\frac{\psi}{a}}\right) \tag{4.5}$$

where ψ undergoes its own time evolution according to

$$\frac{d\psi}{dt} = G(V, \psi) = \frac{bV_0}{D_c}\left(e^{\frac{f_0-\psi}{b}} - \frac{V}{V_0}\right). \tag{4.6}$$

Here f_0 is a reference friction coefficient for steady sliding at slip velocity V_0, a and b are dimensionless parameters characterizing the direct and state evolution effects, respectively, and D_c is the state evolution distance. For commonly used frictional parameters (which we state in Sections 5 and 6.2) and for all values of the state variable ψ, (4.5) satisfies the conditions of Proposition 1. The relevant time scale introduced by friction in Eq. (4.6) is D_c/V, which means we may take large time steps during the interseismic period, when the slip velocity V is quite small.

5. Method of manufactured solutions

In order to test the spatial accuracy of our method as well as the ability to time step quickly through regions characterized by varying time scales we proceed by the method of manufactured solutions [33]. We construct an exact solution to (2.1) and use the exact solution to specify the initial and boundary conditions, as well as source terms. Because we want to be able to capture both the slow loading period as well as the dynamic rupture (fast variations in time), we choose a time dependence for the solution that ranges over many orders of magnitude. For the velocity component of the exact solution, we want the velocity at the fault ($y = 0$) to remain "locked" for a long period of time, that is, at a value close to zero (denoted v_{min}) followed by an "event" or "earthquake" where its value increases over many orders of magnitude to a value v_{max} over a short time scale, as seen in Fig. 3. We also want the stress component to mimic what we often see in simulations where, during this event, the stress drops from a background level σ_b to a lower, residual value σ_r. This event occurs at a time centered at
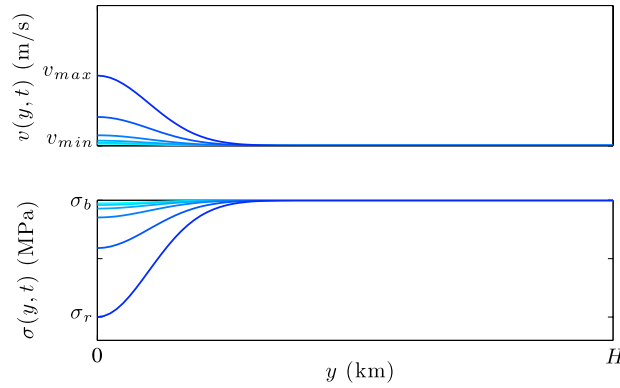
Fig. 4. Velocity $v(y, t)$ and stress $\sigma(y, t)$ from the manufactured solution plotted every 2 min in 10 min period leading up to event time $\bar{t}$. Time increases with darker shades of blue. Essentially at rest $v(y, t) = v_{min}$ during the interseismic period, the system undergoes an event where slip velocity $V(t) = v(0, t)$ increases to a new value v_{max}, and stress at the fault $\sigma(0, t)$ drops from a background value σ_b to a residual value σ_r. (For interpretation of the references to color in this figure legend, the reader is referred to the web version of this article.)

$\bar{t}$ and over a time scale characterized by t_w. The exact solution is given by

$$v(y, t) = R(t)\phi(y) + V_p(1 - \phi(y)) \tag{5.1}$$

$$\sigma(y, t) = -S(t)\phi(y) + \sigma_b \tag{5.2}$$

where

$$R(t) = \frac{v_{max}}{1 + \left(\frac{t - \bar{t}}{t_w}\right)^2} + v_{min}, \qquad S(t) = \frac{(\sigma_b - \sigma_r)}{1 + (\frac{t - \bar{t}}{t_w})^2}, \qquad \phi(y) = \frac{1}{\sqrt{2\pi}y_w}e^{\frac{-y^2}{2y_w^2}}. \tag{5.3}$$

Thus the velocity at the remote boundary remains set at the slow plate rate V_p and during the long interseismic period the velocity at the fault remains at a low value $v_{\min}$, but increases to $v_{\max}$ at which point the velocity profile takes the shape of a Gaussian centered at the fault. The stress mimics this behavior, as seen in Fig. 4.

    The exact solution solves the following problem

$$\frac{\partial w}{\partial t} = B\frac{\partial w}{\partial y} + \begin{bmatrix} f_1(y, t) \\ f_2(y, t) \end{bmatrix}, \quad B = \begin{bmatrix} 0 & 1/\rho \\ \mu & 0 \end{bmatrix}, \quad w = \begin{bmatrix} v \\ \sigma \end{bmatrix}, \ y \in [0, H] \tag{5.4a}$$

$$L_o(w) = \sigma(0, t) = F(V(t), \psi(t)), \qquad L_1(w) = v(H, t) = V_p \tag{5.4b}$$

where again, the slip velocity $V(t) = v(0, t)$. The source terms in (5.4a) are

$$f_1(y, t) = R'(t)\phi(y) + (1/\rho)S(t)\frac{\partial\phi}{\partial y}, \qquad f_2(y, t) = -S'(t)\phi(y) - \mu\left[R(t)\frac{\partial\phi}{\partial y} - V_p\frac{\partial\phi}{\partial y}\right]. \tag{5.5}$$

We must also add a source term to Eq. (4.6). Enforcing boundary conditions at the fault lets us solve for the exact, known solution for the state variable $\psi(t)$:

$$\psi(t) = a\ln\left[\frac{2V_0}{V(t)}\sinh\left(\frac{\sigma(0, t)}{\sigma_n a}\right)\right] \tag{5.6}$$

which we insert into

$$\frac{d\psi}{dt} = G(V, \psi) + s(y, t) \tag{5.7}$$

and solve for the source term $s(y, t)$. Although this manufactured solution does not explicitly generate waves which propagate through the medium, it is sufficiently complex in that it evolves over 12 orders of magnitude for the parameters we consider. We test the spatial accuracy of our method by performing convergence tests with SBP operators of order $p = 2, 4, 6$ and 8, using the time stepping method detailed in Section 4. The SBP operators are order p in the interior of the domain, but due to how they transition to one-sided differences near the boundary, accuracy is lost, and the global order of accuracy obtained is $p/2 + 1$ (i.e. global accuracy of 2, 3, 4 and 5, respectively) [34–39]. Specific values of the parameters used in convergence tests are given in Table 1.

    For the numerical solution $\mathbf{w}$ to Eq. (5.4), we let $\mathbf{w}^*$ denote the exact solution (evaluated at the grid points), and calculate the error in the discrete energy norm defined in (3.5). The error is thus given by

$$E = \|\mathbf{u} - \mathbf{u}^*\|_{\mathbf{P}\otimes\mathbf{l_2}}, \quad \text{where } \mathbf{u} = (I_N \otimes W^{-1})\mathbf{w}, \ \mathbf{u}^* = (I_N \otimes W^{-1})\mathbf{w}^*. \tag{5.8}$$

We expect to see convergence rates of $(p/2) + 1$, due to the lower accuracy at the boundary, see [40]. The convergence results are shown in Table 2.

Table 1

Parameters used in manufactured solution convergence tests.

Parameter	Value	Parameter	Value
H	10 km	V_p	10^{-9} m/s
v_{min}	10^{-12} m/s	v_{max}	1 m/s
$\bar{t}$	10 yr	t_w	100 s
σ_b	30 MPa	σ_r	20 MPa
y_w	$1/\sqrt{2\pi}$ km	V_p	10^{-9} m/s
f_0	0.6	V_0	10^{-6} m/s
a	0.015	b	0.02
c_s	3 km/s	μ	30 GPa
σ_n	100 MPa	D_c	0.2 m

Table 2

Error computed in the discrete energy-norm. We expect to achieve convergence rates of 2, 3, 4, 5 for the 2nd, 4th, 6th and 8th order operators, respectively.

N	E (2nd)	Rate	E (4th)	Rate	E (6th)	Rate	E (8th)	Rate
2^5	1.822×10^{-2}	–	8.850×10^{-3}	–	1.977×10^{-3}	–	1.906×10^{-3}	–
2^6	4.894×10^{-3}	1.897	1.204×10^{-3}	2.877	8.913×10^{-5}	4.471	8.584×10^{-5}	4.473
2^7	1.099×10^{-3}	2.155	1.452×10^{-4}	3.052	3.997×10^{-6}	4.478	3.005×10^{-6}	4.836
2^8	2.833×10^{-4}	1.955	1.754×10^{-5}	3.048	2.080×10^{-7}	4.264	9.043×10^{-8}	5.054
2^9	7.106×10^{-5}	1.995	2.166×10^{-6}	3.018	1.063×10^{-8}	4.290	2.833×10^{-9}	4.996
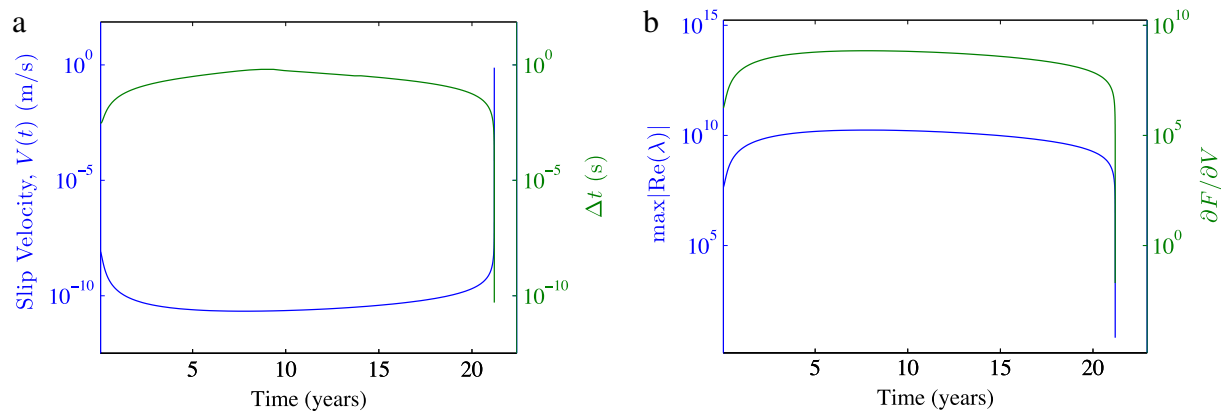
Fig. 5. (a) During a cycle consisting of an interseismic period (when slip velocity $V(t) \ll 1$ mm/s) followed by a dynamic event, our method integrates efficiently through both periods. Large time steps are taken during the slow loading period until the event takes place and the time step reduces to ~fractions of a second in order to fully resolve rupture. (b) During the same cycle, we calculate the Jacobian matrix of the system at each time step for the full, nonlinear friction law. Here we show that during the interseismic period, this eigenvalue assumes absolute values of around 10^8–10^{10}, and decreases abruptly during rupture. The eigenvalue is influenced directly by the partial derivative of the friction law $\partial F/\partial V$.

6. Application problem

Having verified that our numerical method converges to the true solution under mesh-refinement, we apply our time-stepping method to solve Eq. (2.1) in order to simulate multiple earthquake cycles.

6.1. Stiffness in the interseismic and dynamic rupture periods

Our implicit time-stepping method is capable of efficiently integrating through both the interseismic loading period as well as the dynamic rupture itself, with the full, nonlinear friction law given by Eq. (4.5). Fig. 5(a) shows slip velocity and time step during the interseismic period (when slip velocity $V(t) \ll 1$ m/s) and during the dynamic rupture period where the slip velocity increases over 10 orders of magnitude. The time step is quite large during the slow loading period, and adapts accordingly in order to resolve rupture.

As pointed out in Section 4.1, a linearized friction law of the form $F(V) = \alpha V$, was shown to introduce stiffness in single event simulations (modeling just the earthquake itself) due to the fact that $\alpha = \partial F/\partial V$ was seen to range over many orders of magnitude. We calculate the Jacobian matrix of the right hand side of Eq. (2.1) with the full non-linear friction law and with state variable evolution given by Eq. (4.6). As shown in Fig. 5(b), the Jacobian matrix exhibits an eigenvalue with large (negative) real part on the order of 10^{10} during the interseismic period for commonly used frictional parameters, listed in Table 3. During the earthquake itself, the real part of the eigenvalue drops to values on the order of 10^2, suggesting

Table 3
Parameters used in model application problem.

Parameter	Value	Parameter	Value
H	10 km	V_p	10^{-9} m/s
f_0	0.6	V_0	10^{-6} m/s
a	0.015	b	0.02
σ_n	50 (MPa)	D_c	8 mm
μ	36 GPa	c_s	3 km/s

that in addition to the dynamic rupture period, stiffness is even greater during the interseismic period. Fig. 5(b) echoes the linearized analysis, in that the relevant eigenvalue of the Jacobian matrix depends directly on the partial derivative $\partial F/\partial V$, which ranges over 10 orders of magnitude during the cycle. While explicit time-stepping methods with a very small time step ($\sim$fractions of a second) in order to maintain stability might be able to integrate efficiently through the short rupture period ($\sim$seconds), to use them to simulate the interseismic period ($\sim$100 years) with any efficiency is not possible.

6.2. The multiple-penalty technique for an absorbing boundary

In order to apply our method to a model problem and generate multiple events in our simulation, we need a technique for deriving non-reflecting boundary conditions so that waves emitted at the fault do not reflect off the remote boundary. We do this through the use of the so-called multiple-penalty technique, which will draw the velocity of the outgoing wave at the remote boundary towards the slow plate rate V_p. This technique is described in detail in [41]. The semi-discrete form of the Eqs. (2.1) with m additional penalty matrices is

$$(P \otimes I_2)\mathbf{w}_t = (Q \otimes B)\,\mathbf{w} + \left(e_0 \otimes \Sigma_0 \begin{bmatrix} \sigma_0 - F(v_0) \\ \sigma_0 - F(v_0) \end{bmatrix}\right) + \left(e_N \otimes \Sigma_N \begin{bmatrix} v_N - V_p \\ v_N - V_p \end{bmatrix}\right)$$

$$+ \sum_{j=1}^{m} \left(e_{N-j} \otimes \Sigma_{N-j} \begin{bmatrix} v_{N-j} - V_p \\ v_{N-j} - V_p \end{bmatrix}\right). \tag{6.1}$$

The penalty matrices will be determined such that we get a discrete energy estimate. It can be shown by similar analysis through the discrete energy method that the additional penalty matrices are

$$\Sigma_{N-j} = \begin{bmatrix} \beta_j & 0 \\ 0 & 0 \end{bmatrix}, \quad \beta_j \le 0, \; j = 1, 2, \ldots, m \tag{6.2}$$

and lead to a stable scheme if $\beta_j \le 0$. In summary, the approximation (6.1) of (2.1) in combination with (6.2) is stable. To test this technique, we apply our time-stepping technique outlined in Section 4 to the semi-discrete equation given in (6.1). The model parameters used are listed in Table 3.

We take $\beta_j = -1$ for $j = 1, 2, \ldots, m$, where m is the number of penalties in the vicinity of $y = H$. For this simulation we take $N = 400$, and $m = 80$, corresponding to a penalty domain of 2 km. The penalties β_j are turned on when the wave hits the remote boundary, damping the outgoing wave (see [41] for more details).

As seen in Fig. 6, the system initially undergoes an interseismic period lasting $\sim$125 years, where the fault remains essentially locked with slip velocities lower than 10^{-15} m/s. The system is loaded at the remote boundary at the rate $V_p = 32$ mm/yr which increases the stress on the fault until an earthquake nucleates at which point slip velocity increases over 10 orders of magnitude during one of these dynamic events. These events nucleate periodically every $\sim$125 years, each event sending a wave from the fault and through the medium. The multiple penalties damp this outgoing wave and another interseismic period ensues. The time-stepping method outlined in Section 4 adapts appropriately, with long time steps taken during the interseismic period followed by very small time-steps during each earthquake in order to resolve wave propagation during rupture, as illustrated in Figs. 3 and 5(a). The method is extremely efficient and allows for the simulation of the full earthquake cycle where initial conditions are generated from capturing the effect of slow, tectonic loading. The interseismic period and the dynamic rupture itself are characterized by vastly different time scales and our method incorporates both regimes within a single computational framework.

7. Conclusions

We have derived a provably stable, high-order accurate discretization to the elastic wave equation and used an A- and L-stable time-stepping method capable of integrating through regimes characterized by time scales that vary over many orders of magnitude. The stiffness of the problem is present during the interseismic loading period in addition to the dynamic rupture, thus explicit methods cannot be used. Our method efficiently handles stiffness and multi-scale temporal features, taking large time steps during the interseismic period and adapting the time-step accordingly when an earthquake nucleates.

We have tested our numerical method through the method of manufactured solutions and shown that the numerical solution converges to the true solution at the appropriate rate. Finally, we have utilized the multiple-penalty technique that
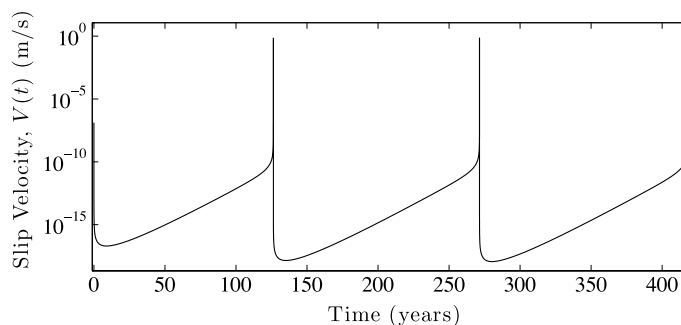
Fig. 6. Slip velocity V as a function of time for the application problem. Large time steps are taken during the interseismic period lasting approximately 150 years. Periodic events nucleate during which slip velocity increases over 15 orders of magnitude.

mimics a non-reflecting boundary in order to effectively damp outgoing waves. Rather than imposing artificial initial conditions, our method generates multiple cycles of earthquakes with self-consistent initial data obtained through interseismic loading.

Acknowledgments

References

[1] E.M. Dunham, D. Belanger, L. Cong, J.E. Kozdon, Earthquake ruptures with strongly rate-weakening friction and off-fault plasticity, part 1: planar faults, BSSA 101 (5) (2011) 2296–2307.
[2] J.E. Kozdon, E.M. Dunham, Rupture to the trench: dynamic rupture simulations of the 11 March 2011 Tohoku earthquake, Bull. Seismol. Soc. Am. 103 (2B) (2013) 1275–1289.
[3] Z. Shi, S.M. Day, Rupture dynamics and ground motion from 3-D rough-fault simulations, J. Geophys. Res. 118 (3) (2013) 1122–1141.
[4] P.G. Okubo, Dynamic rupture modeling with laboratory-derived constitutive relations, J. Geophys. Res. 94 (1989) 12321–12335.
[5] B. Shibazaki, M. Matsu'ura, Spontaneous processes for nucleation, dynamic propagation, and stop of earthquake rupture, J. Geophys. Res. 101 (1996) 13911–13917.
[6] B.A. Erickson, E.M. Dunam, An efficient numerical method for earthquake cycles in heterogeneous media: alternating subbasin and surface-rupturing events on faults crossing a sedimentary basin, J. Geophys. Res. (2014).
[7] L. Lapusta, J. Rice, Y. Ben-Zion, G. Zheng, Elastodynamic analysis for slow tectonic loading with spontaneous rupture episodes on faults with rate-and-state depended friction, J. Geophys. Res. 105 (B10) (2000) 23765–23789.
[8] H.O. Kreiss, J. Oliger, Comparison of accurate methods for the integration of hyperbolic equations, Tellus 24 (1972) 199–215.
[9] D.W. Zingg, Comparison of high-accuracy finite-difference methods for linear wave propagation, SIAM J. Sci. Comput. 22 (2) (2001) 476–502.
[10] H.O. Kreiss, G. Scherer, Finite element and finite difference methods for hyperbolic partial differential equations, in: Mathematical Aspects of Finite Elements in Partial Differential Equations, Academic Press, Inc., 1974.
[11] H.O. Kreiss, G. Scherer, On the Existence of Energy Estimates for Difference Approximations for Hyperbolic Systems, Technical Report, Department of Scientific Computing, Uppsala University, 1977.
[12] Bo Strand, Summation by parts for finite difference approximations for d/dx, J. Comput. Phys. 110 (1) (1994) 47–67.
[13] M.H. Carpenter, J. Nordström, D. Gottlieb, A stable and conservative interface treatment of arbitrary spatial accuracy, J. Comput. Phys. 148 (1999) 341–365.
[14] B. Gustafsson, H.O. Kreiss, J. Oliger, Time Dependent Problems and Difference Methods, Wiley–Interscience, New York, 1995.
[15] P. Olsson, Summation by parts, projections, and stability, I, Math. Comp. 64 (211) (1995) 1035–1065.
[16] P. Olsson, Summation by parts, projections, and stability, II, Math. Comp. 64 (212) (1995) 1473–1493.
[17] K. Mattsson, Boundary procedures for summation-by-parts operators, J. Sci. Comput. 18 (1) (2003) 133–153.
[18] M.H. Carpenter, J. Nordström, D. Gottlieb, Revisiting and extending interface penalties for multi-domain summation-by-parts operators, J. Sci. Comput. 45 (1–3) (2010) 118–150.
[19] J. Gong, J. Nordström, Interface procedures for finite difference approximations of the advectiondiffusion equation, J. Comput. Appl. Math. 236 (5) (2011) 602–620.
[20] M.H. Carpenter, D. Gottlieb, S. Abarbanel, Time-stable boundary conditions for finite-difference schemes solving hyperbolic systems: methodology and application to high-order compact schemes, J. Comput. Phys. 111 (2) (1994) 220–236.
[21] J. Nordström, M.H. Carpenter, Boundary and interface conditions for high-order finite-difference methods applied to the Euler and Navier–Stokes equations, J. Comput. Phys. 148 (2) (1999) 621–645.
[22] J. Nordström, M. Svärd, Well posed boundary conditions for the Navier–Stokes equations, SIAM J. Numer. Anal. 43 (3) (2005) 1231–1255.
[23] D.J. Bodony, Accuracy of the simultaneous-approximation-term boundary condition for time-dependent problems, J. Sci. Comput. 43 (1) (2010) 118–133.
[24] M. Svärd, J. Nordström, Review of summation-by-parts schemes for initial–boundary-value problems, J. Comput. Phys. 268 (2014) 17–38.
[25] U.M. Ascher, L.R. Petzold, Computer Methods for Ordinary Differential Equations and Differential–Algebraic Equations, first ed., SIAM, 1998.
[26] J.E. Kozdon, E.M. Dunham, J. Nordström, Interaction of waves with frictional interfaces using summation-by-parts difference operators: weak enforcement of nonlinear boundary conditions, J. Sci. Comput. 50 (2012) 341–367.
[27] J. Nordström, Linear and nonlinear boundary conditions for wave propagation problems, in: Notes on Numerical Fluid Mechanics and Multidisciplinary Design, vol. 120, 2013.
[28] B. Strand, Summation by parts for finite difference approximations for d/dx, J. Comput. Phys. 110 (1994) 47–67.

[29] J. Dieterich, Time-dependent friction and the mechanics of stick–slip, Pure Appl. Geophys. 116 (1978) 790–806.
[30] J.H Dieterich, Modeling of rock friction, 1, experimental results and constitutive equations, J. Geophys. Res. 84 (1979) 2161–2168.
[31] J.H. Dieterich, B.D. Kilgore, Direct observation of frictional contacts: new insights for state dependent properties, Pure Appl. Geophys. 143 (1994) 283–302.
[32] C. Marone, Laboratory-derived friction laws and their application to seismic faulting, Annu. Rev. Earth Planet. Sci. 26 (1998) 643–696.
[33] P.J. Roache, Verification and Validation in Computational Science and Engineering, first ed., Hermosa Publishers, Albuquerque, 1998.
[34] M. Svärd, J. Nordström, On the order of accuracy for difference approximations of initial–boundary value problems, J. Comput. Phys. 218 (2006) 333–352.
[35] J. Nordström, J. Berg, Conjugate heat transfer for the unsteady compressible Navier–Stokes equations using a multi-block coupling, Comput. & Fluids 72 (2013) 20–29.
[36] M. Svärd, J. Lundberg, J. Nordström, A computational study of vortex–airfoil interaction using high-order finite difference methods, Comput. & Fluids 39 (2010) 1267–1274.
[37] D. Amsallem, J. Nordström, High-order accurate difference schemes for the Hodgkin–Huxley equations, J. Comput. Phys. 252 (2013) 573–590.
[38] J. Nordström, J. Gong, E. van der Weide, M. Svärd, A stable and conservative high order multi-block method for the compressible Navier–Stokes equations, J. Comput. Phys. 228 (2009) 9020–9035.
[39] J. Nordström, R. Gustafsson, High order finite difference approximations of electromagnetic wave propagation close to material discontinuities, J. Sci. Comput. 18 (2003) 215–234.
[40] M. Svärd, J. Nordström, On the order of accuracy for difference approximations of initial–boundary value problems, J. Comput. Phys. 218 (1) (2006) 333–352.
[41] J. Nordström, Q. Abbas, B.A. Erickson, H. Frenander, A flexible boundary procedure for hyperbolic problems: multiple penalty terms applied in a domain, Comm. Comput. Phys. (2014) in press.